Ultrafast Dynamics of Resonance Energy Transfer in Myoglobin: Probing Local Conformation Fluctuations

Jeffrey A. Stevens, Justin J. Link,[†] Ya-Ting Kao, Chen Zang, Lijuan Wang, and Dongping Zhong*

Departments of Physics, Chemistry, and Biochemistry, OSU Biophysics, Chemical Physics, and Biochemistry Programs, 191 West Woodruff Avenue, The Ohio State University, Columbus, Ohio 43210

Received: October 19, 2009; Revised Manuscript Received: November 23, 2009

We report here our systematic characterization of resonance energy transfer between intrinsic tryptophan and the prosthetic heme group in myoglobin in order to develop a novel energy-transfer pair as a molecular ruler in heme proteins to study local conformation fluctuations. With site-directed mutagenesis, we designed four tryptophan mutants along the A-helix of myoglobin and each mutant contains only a single tryptophan−heme energy-transfer pair. With femtosecond resolution, we observed, even at separation distances of 15−25 Å, ultrafast energy transfer in tens to hundreds of picoseconds. On these time scales, the donor and acceptor cannot be randomized and the orientation factor in Förster energy transfer is highly restricted. Thus, direct measurement of the orientation-factor changes at different mutation sites reveals relative local structure flexibility and conformation fluctuations as particularly demonstrated here for positions of tryptophan 7 and 14. More importantly, the local environment relaxation occurs on the similar time scales of the energy transfer dynamics, resulting in a nonequilibrium dynamic process. With femtosecond- and wavelength-resolved fluorescence dynamics, we are able to determine the time scales of such nonequilibrium energy-transfer dynamics and elucidate the mechanism of the nonexponential energy-transfer dynamics caused by local dynamic heterogeneity and/or local environment relaxation.

I. Introduction

Protein fluctuation is a central determinant to many biological activities and especially essential to its biological recognitions and reactions,[1−9] such as serum albumins,[4,5] calmodulins,[6,7] and kinases[8,9] which all have a remarkable plasticity to adopt distinct conformations in binding sites or catalytic domains for various drug transports and signaling pathways. The direct characterization of these conformational changes has been challenging,[10−14] especially for motions occurring on picosecond (ps) to nanosecond (ns) time scales.[13,14] On these fast time scales, the local conformational fluctuations are dominant. One typical experimental strategy is to introduce a perturbation by instantaneous temperature jump,[15−17] electron transfer,[18] bond breaking,[19,20] or isomerization,[21] to shift the initial equilibrium configuration to a nonequilibrium state, and then follow temporal evolution of the system's relaxation. To quantify these local conformation motions, we need a site-specific molecular reporter to probe local relaxation[13,22−24] or a molecular ruler to measure relative distance fluctuations.[14,25,26] Resonance energy transfer (RET) is very sensitive to distance changes and has been widely used to study protein dynamics by labeling extrinsic dye molecules to a protein's specific sites.[27−29] Here, we develop an intrinsic energy-transfer pair, without extrinsic labeling, using natural amino acid tryptophan and prosthetic heme group to probe local conformation fluctuations in heme proteins.

Myoglobin (Mb) from sperm whale, a well-studied globular protein, is chosen as a model system. The X-ray structure[30] is shown in Figure 1 and the protein has eight α-helices (A-H) with a total of 153 amino acids. The two intrinsic tryptophan residues, W7 and W14, are located in the A-helix near the N-terminal. The center-to-center distance is 21.2 Å from W7 to the heme and 15 Å for W14. These distances are much larger than the molecular dimensions of tryptophan and the heme and the energy-transfer pair is well separated. Thus, the energy-transfer kinetics follows the Förster resonance energy-transfer rate equation within the point−dipole approximation.[31−33] Earlier studies have observed the RET process between tryptophan and the heme in several proteins of hemoglobin,[34] peroxidase,[35] and myoglobin.[36−38] Hochstrasser and Negus[36] first measured the energy-transfer kinetics in ferric Mb and reported a time scale of 20 ps for W14 and 130 ps for W7. Szabo and co-workers[38] later performed more detailed studies with different binding

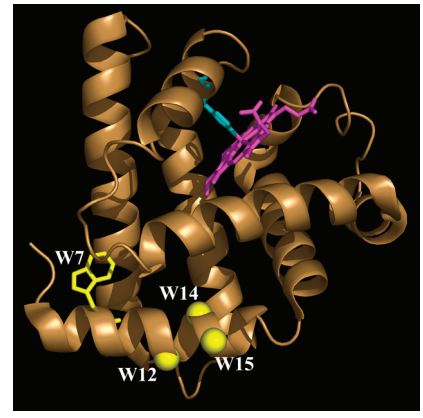

Figure 1. X-ray crystallographic structure of holo-myoglobin[30] (PDB 1MBD) with four mutation positions of W7, W12, W14, and W15 in yellow as the energy donor along the A helix. Also shown is the energy acceptor of the prosthetic heme group in pink.

* Corresponding author. Phone: (614)292-3044. Fax: (614)292-7557. E-mail: dongping@mps.ohio-state.edu.
[†] Present address: Department of Physics, Xavier University, Cincinnati, OH 45207.

10.1021/jp910013f
Published on Web 01/04/2010

ligands, iron redox states, and pH values and refined the RET kinetics of W14 in 21.5 ps and W7 in 112.5 ps in ferric Mb. Bucci and co-workers[39] did careful analyses of the orientation factor (κ^2) in the Förster energy-transfer equation for both W7 and W14 to rationalize the observed kinetic results.

In this study, we first use protein engineering to mutate out one tryptophan in Mb and make each mutant (W14Y and W7Y) with only a single tryptophan of W7 or W14. We also design another two mutants with W12 and W15 by triple mutations of W7YH12WW14F and W7YW14FA15W (Figure 1).[40] All four mutants in the A-helix have a single tryptophan−heme energy transfer pair. We then carefully characterize their quantum yields, fluorescence lifetimes, and spectral overlap integrals. Using the same tryptophan residues at these four sites, we have recently studied the local hydration dynamics and their wobbling motions.[41] All these relaxations occur on the time scales of picoseconds, as does the tryptophan−heme energy transfer. Thus, the RET here is a nonequilibrium process.[33] With femtosecond (fs)- and wavelength-resolved fluorescence transients, we are able to determine the RET dynamics precisely. With molecular dynamics (MD) simulations, we examine the fluctuations of relative distances and orientations of tryptophan and the heme, and directly compare MD results with experimental observations. Finally, we examine the RET changes with temperature and probe the local conformational fluctuations at different sites.

II. Experimental Section

A. Femtosecond Laser Setup. All of the femtosecond-resolved measurements were carried out by using a fluorescence up-conversion method. The integrated experimental setup has been described elsewhere.[42] Briefly, the femtosecond pulse after the two-stage amplifier (Spitfire; Spectra-Physics) has a temporal width of 110 fs centered at 800 nm with an energy of more than 2 mJ per pulse and a repetition rate of 1 kHz. Half of the laser energy was used to pump an optical parametric amplifier (OPA-800C; Spectra-Physics) to generate signal (1289 nm) and idler (2109 nm) beams. The latter was mixed with the residual fundamental (800 nm) in a 0.2 mm thick β-barium borate (BBO) crystal (type I) to generate a femtosecond pulse at 580 nm. This femtosecond pulse was frequency-doubled to generate our pump wavelength at 290 nm by another 0.2 mm thick BBO crystal. The pump pulse energy typically was attenuated to 100−140 nJ per pulse before being focused into the motor-controlled rotating sample cell. The fluorescence emission was collected by a pair of parabolic mirrors and mixed with a gating pulse from another half of the fundamental beam (attenuated) in a 0.2 mm BBO crystal through a noncollinear configuration. The up-converted signal ranging from 223 to 253 nm was detected by a photomultiplier coupled with a double-grating monochromator. The instrument response time under the current noncollinear geometry is about 400−500 fs as determined from the up-conversion signal of Raman scattering of water at 320 nm. For all studies, the pump-beam polarization was set at a magic angle (54.7°) with respect to the acceptance axis (vertical) of the up-conversion crystal, and the polarization of the gating beam was set parallel to this axis through a half-wave plate.

B. Sample Preparation. The mutant design and purification of Mb have been described in detail elsewhere.[40,43] To achieve single tryptophan to heme RET, site-directed mutagenesis was used to place one tryptophan residue in each mutant. The plasmid pMb122, containing the sperm whale myoglobin gene, was used to mutate tryptophan to tyrosine one at a time on the two intrinsic tryptophan residues, W7 and W14, in the A-helix

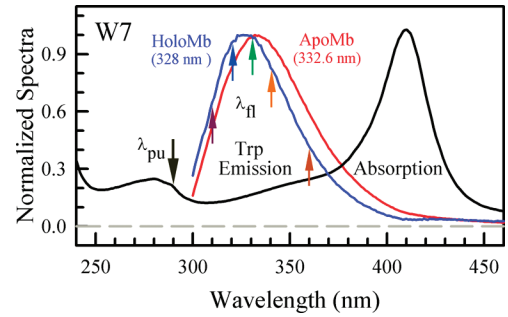

Figure 2. Normalized absorption and emission spectra of a typical mutant (W7) holoMb. Also shown is the fluorescence emission of the corresponding apoMb. Note that the emission peak in holoMb is bluer than that in apoMb. The arrows mark the pump wavelength (λ_{pu}) and the typical gated fluorescence wavelengths (λ_{fl}).

to W7Y (W14) and W14Y (W7). To place a single tryptophan at positions 12 and 15, we first mutated out both tryptophans (W7 and W14) and the double mutation of W7YW14F was used as a template[44] for the triple mutants of W7YH12WW14F and W7YW14FA15W. All of the mutants were expressed in *Escherichia coli* with a reasonable yield. ApoMb was prepared by removing the prosthetic heme group according to the standard procedure,[45] and all apoMb mutants were screened for their tryptophan's lifetimes to make sure no ultrafast quenching from neighboring protein residues.[46] All holoMb samples were dissolved in 20 mM Tris and 1 mM EDTA at pH 7.5 and apoMb was dissolved in the buffer of 10 mM sodium acetate at pH 6.1. The structures of apoMb mutants were examined by their CD spectra to verify the appropriate folding.[40] Quantum yield measurements were performed at dilute concentrations of less than 10 uM in a 1 cm quartz cuvette. DeoxyMb was prepared by purging the ferric protein with high-purity nitrogen to remove oxygen and then reducing it with a 1:5 ratio of protein to sodium dithionate.[47] MbCO was prepared from deoxyMb by purging the sample with CO for ~1 min. All protein concentrations were maintained at ~200 uM and all femtosecond-resolved experiments were done in either a 1 mm quartz rotation cell or a 1 mm quartz moving cuvette to avoid sample heating and degradation. All temperature-dependent measurements were performed in a 1 mm rotation cell that was heated and cooled with a VWR water-bath circulator. To ensure that there were no changes in iron redox states, ligand binding, and protein quality, the absorption spectra of each sample were verified before and after time-resolved measurements. Figure 2 shows a typical absorption spectrum of ferric holoMb and tryptophan emission spectra of both ferric holoMb and apoMb of the W7 mutant.

III. Results and Discussion

A. Ultrafast Fluorescence Dynamics and Resonance Energy Transfer. A series of wavelength-resolved fluorescence transients was taken from the blue to red side of the emission spectra for four mutants in both apoMb and holoMb and Figure 3 shows several typical transients of W7 in two forms. In apoMb, the emission peak of W7 is 332.6 nm (Figure 2) and all the transients at the blue side of the peak in Figure 3B show two ultrafast solvation relaxations and two long-lifetime decays. The two solvation dynamics are in 5 and 87 ps and the two lifetimes are 1 and 4.6 ns.[40,41] At the red side of the emission peak, the transients decay by two long-lifetime emissions. In ferric holoMb, all the transients become much faster as shown in Figure 3A. Such changes must result from the RET from excited tryptophan to the heme group, not from any other protein

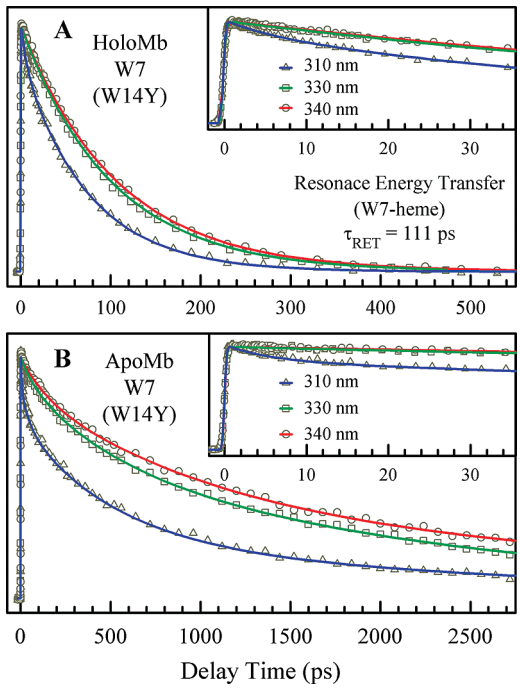

Figure 3. Normalized, femtosecond-resolved fluorescence transients of W7 (W14Y) mutant in holoMb (A) and apoMb (B) with a series of gated fluorescence emissions. The transients in short-time range are shown in insets. In holoMb, a minor long component (1−3%) was removed for clarity. Note the different time scales of the two panels and in holoMb the transients decay much faster.

side chain quenching.[46] Similarly, at the blue side, the dynamics results from a mixture of solvation relaxation and energy transfer. At the red side, the fast decay is dominant and from the RET process. For W7, the red-side signal can be fit by a dominant single-exponential decay with a time constant of 111 ps (Figure 3A). Thus, to study the RET dynamics and determine its time scale (rate) accurately under the nonequilibrium state, we must detect the time-resolved fluorescence dynamics at the emission peak or longer wavelengths.

Similarly, we studied three other mutants and the results are shown in Figure 4. The RET dynamics are obtained by gating the red-side emission. For W14, the RET dynamics follows a single-exponential decay in 22 ps (Figure 4A) and for W12, the dynamics becomes much slower with a dominant decay in 212 ps (Figure 4B). However, for the W15 mutant, the transient at the red side clearly does not follow a single-exponential decay and the signal can be fit by at least three exponential decays, 3.3 ps (16%), 94 ps (58%), and 390 ps (25%), or a stretched single-exponential decay of $e^{-(t/\tau)^{\beta}}$ with 120 ps (τ) and 0.67 (β). The average time scale ($<\tau>$) is about 158 ps. Such multiple or stretched decay behaviors could reflect significant dynamic heterogeneity of W15 mutant and the dominant single-exponential decays of the other three mutants would suggest a less extent of heterogeneity. Figure 4C shows a comparison of the RET dynamics of these three mutants. The four mutants, W7, W12, W14 and W15, on the A-helix exhibit very different RET dynamics in 111, 212, 22, and 158 ps, respectively. Because the nanosecond lifetime contributions are negligible, the obtained time scales truly reflect the RET dynamics. In the following, we evaluate various parameters for determination of the RET time scales and examine the dynamic heterogeneity.

At the point−dipole approximation, the Förster resonance energy-transfer rate equation through dipole−dipole interaction at equilibrium state is given below[48]

$$k_{RET} = \frac{1}{\tau_D}\left(\frac{R_0}{r}\right)^6 = 8.79 \times 10^{23}\frac{\kappa^2 Q_D J}{\tau_D n^4 r^6} \qquad \text{(III.1)}$$

where Q_D and τ_D are the donor's fluorescence quantum yield and lifetime in picoseconds without the energy acceptor, respectively, J is the spectral overlap integral of the normalized donor fluorescence spectrum and the acceptor's absorption spectrum expressed by its extinction coefficient in units of cm^3 M^{-1}, n is the refractive index, which usually is ~1.33 in the protein,[49] and r is the center-to-center distance of the donor and acceptor in Å. The orientation factor κ^2 is related to the relative alignments of the donor and the acceptor. For a given X-ray structure for W7 and W14 and with MD simulations for W12 and W15, we know the distance of r in eq III.1. Thus, we need to measure the quantum yields (Q_D), lifetimes (τ_D), and fluorescence spectra for calculations of J in apoMb without the acceptor heme group. Using tryptophan's quantum yield of 0.14 in water as control, we obtained quantum yields (Q_D) of 0.20 and 0.17 for W7 and W14, respectively. These numbers are larger than the reported values of ~0.08−0.1 in the literature,[50] and we should point out here that caution must be taken when measuring the apoMb concentration. It is extremely easy to overestimate the apoMb concentration due to UV scattering in the absorption spectrum, resulting in underestimate of the quantum yield. Also, the emission spectra were taken at a very

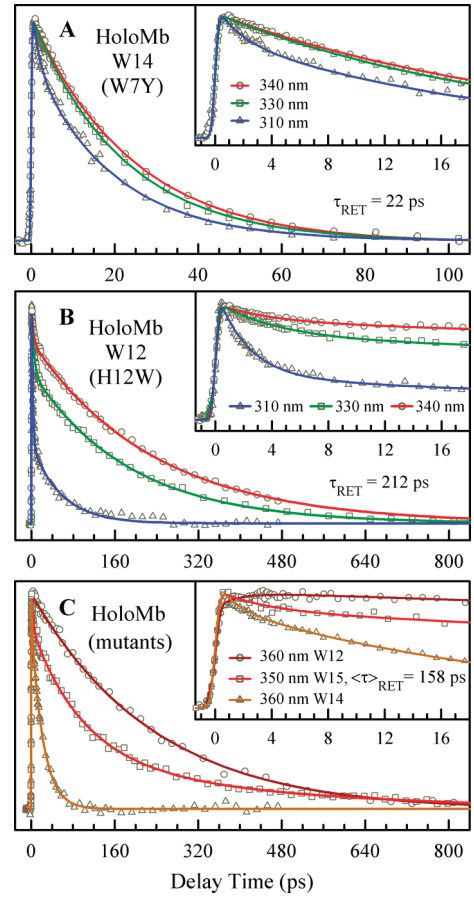

Figure 4. Normalized, femtosecond-resolved fluorescence transients of W14 (A) and W12 (B) mutants in holoMb with a series of gated fluorescence emissions. The mutant W15 is shown in panel C with a comparison of other two mutants at the red-side wavelengths to show different energy-transfer dynamics. All insets show the short-time dynamic behaviors. Note that a small long-lifetime component of less than 20% was removed for clarity.

TABLE 1: Resonance Energy Transfer Times and Related Parameters for W7 and W14

						orientation factor (κ^2)[c]		
mutant	τ_{RET} (ps)[a]	Q_D	J (cm^3 M^{-1})[b]	$\langle\tau_D\rangle$ (ns)	r (Å)	expt	crystal struct	MD
W7	111	0.20	4.47×10^{-14}	2.8	21.2	0.91	0.16	0.16
W14	22	0.17	3.75×10^{-14}	2.6	15.0	0.76	0.73	0.66

[a] With consideration of the nanosecond lifetime contributions, the τ_{RET} values would change to ~115 and 22.2 ps for W7 and W14, respectively, which would not cause noticeable changes of κ^2 values. [b] The J values were calculated using the fluorescence emission peaks of 328 and 324 nm for W7 and W14, respectively. [c] The experimental κ^2 value was calculated using the X-ray distances (r) in the table and the MD κ^2 value was averaged over 19-ns simulations.

dilute concentration of less than 10 μM to make sure that the fluorescence intensity is within the linear region of the fluorescence spectrometer. The lifetimes of W7 and W14 have been measured,[40] similar to the reported values,[51] and the average lifetimes (τ_D) are 2.8 and 2.6 ns, respectively. The resulting radiation lifetime, τ_D/Q_D, is about 14−15 ns for both buried tryptophan residues, consistent with the previous observation for tryptophan in a hydrophobic environment.[52]

To evaluate the spectral overlap integral of J, we must carefully consider the nonequilibrium RET process because the local hydration dynamics around the four mutants occur on the similar time scales. For W7, the weak emission spectrum in holoMb peaks at 328.0 nm, shorter than 332.6 nm in apoMb (Figure 2). The hydration dynamics occur in two distinct time scales of 5 and 87 ps with 245 and 414 cm^{-1} stabilization energy, respectively.[40,41] The emission peak at time zero is 322.0 nm,[40,41] and after the first relaxation in 5 ps, the peak shifts to 324.6 nm. In the following 87 ps relaxation and 111 ps RET process, the final steady-state emission peak ends at 328.0 nm, not 332.6 nm. Thus, during the RET process, the fluorescence spectrum is shifting (Stokes shift) due to the solvation and the J value is changing. If the J value changes significantly, we can also observe a non-single-exponential decay RET dynamics. For W7, we obtained a J value of 4.47×10^{-14} cm^3 M^{-1} with a fluorescence emission peak at 328.0 nm and if we used the peak at 324.6 nm after the first relaxation, the J value would be 4.14×10^{-14} cm^3 M^{-1} but has no significant change. For W14, the fluorescence emission peak in both holoMb and apoMb is 327.0 nm. However, the hydration relaxation occurs in 8.3 and 103 ps with 178 and 371 cm^{-1} stabilization energy, respectively, with a time-zero emission peak at 321.0 nm. The RET process is ultrafast in 22 ps and much faster than the second slower hydration dynamics. Thus, during the RET process, the fluorescence emission peak must be smaller than 327.0 nm. Interestingly, for W7 we observed that the transients at the red side of the emission peak all nearly decay to zero in 111 ps but, for W14, besides the dominant 22 ps decay we also observed a 10−20% long-lifetime component (the origin of this long component will be discussed below). Thus, the steady-state emission in holoMb is mainly from this long component contribution, resulting in the same emission peak as in apoMb. Considering the 22 ps RET process, we estimate from the hydration Stokes shifts[40,41] that the emission peak in holoMb at most shifts from 321.0 nm ($t = 0$) to 324.0 nm and the resulting J value is 3.75×10^{-14} cm^3 M^{-1}. Both J values for W7 and W14 are smaller than the reported values[39] that used the longer-wavelength steady-state apoMb emission spectra, resulting in better spectral overlaps and larger J values.

For W12 and W15, their emission peaks in holoMb are at 337.0 and 342.0 nm, respectively, indicating that both tryptophan residues are more exposed to the surface, consistent with the X-ray structure. The hydration dynamics along the A-helix occur within ~100 ps, and the emission peaks of all tryptophan mutants at time zero in apoMb are about 320.0 nm.[40,41] Thus, for W12 and W15, during the RET processes, the time-resolved emission spectra shift from 320.0 nm to 337.0 and 342.0 nm, respectively. Such nonequilibrium processes and large spectra shifts could result in significantly different J values (see below) during the RET. Besides the possible dynamic heterogeneity of the local structures, the nonequilibrium RET due to the changing of J values could also result in the observed non-single-exponential decay of the fluorescence transients as observed in W15 and W12. However, the apoMb emission peaks of W12 and W15 are at 328.3 and 327.7 nm, respectively, which are largely blue-shifted compared to their holoMb emissions, clearly indicating that the local structures are changed in apoMb and both tryptophan residues become buried inside the protein, similar to W14, resulting from the rotating of the A-helix as also suggested by others.[44] Such structure changes prevent us from further measuring the accurate quantum yields (Q_D), lifetimes (τ_D), emission spectra, and hydration dynamics of apoMb that has the same local structure of holoMb. Thus, we will focus on our analyses and studies below only on W7 and W14.

B. Orientation Factor and Local Structure. Knowing the RET rates, k_{RET}, and all parameters of Q_D, τ_D, r, and J as summarized in Table 1, we can use the Förster eq III.1 to derive the orientation factor κ^2. For W7 and W14, we obtained the κ^2 values of 0.91 and 0.76, respectively. Both values are larger than the averaged value of orientation factor (0.67),[48] which is widely used for Förster energy-transfer studies. Clearly, in most proteins, due to structure constrains the donor and acceptor can be highly restricted and the κ^2 value can be very different from 0.67. Because the κ^2 value can vary from 0 to 4, using the RET to estimate the donor−acceptor distance should be very careful because the significant deviation from 0.67 of the orientation factor could result in a large distance difference. For example, if the κ^2 was 0.1 or 4 but we used the averaged value of 0.67, the resulting distance r ($r \propto (\kappa^2)^{1/6}$) would have a 37% increase or 35% decrease of the original true distance.

With the X-ray structure, the κ^2 value can also be calculated by the following equation[48]

$$\kappa^2 = (\cos\theta_{DA} - 3\cos\theta_D\cos\theta_A)^2 \qquad \text{(III.2)}$$

All angles of θ_{DA}, θ_D, and θ_A are relative orientations as shown in Figure 5A. The transition dipole moment of tryptophan is taken from the ^1L_a transition, 38° from the major axis of the tryptophan ring.[53] The heme transition moment is taken to be in the interval of 50°−60° relative to the α−γ-meso axis of the porphyrin ring.[39] These transition directions are also shown in Figure 5A. In an attempt to observe the variability of κ^2 on the heme transition dipole orientation, κ^2 is calculated for transition moments ranging from 0° to 90° for the normal heme (N) and from 0° to −90° for the disordered heme (D), which

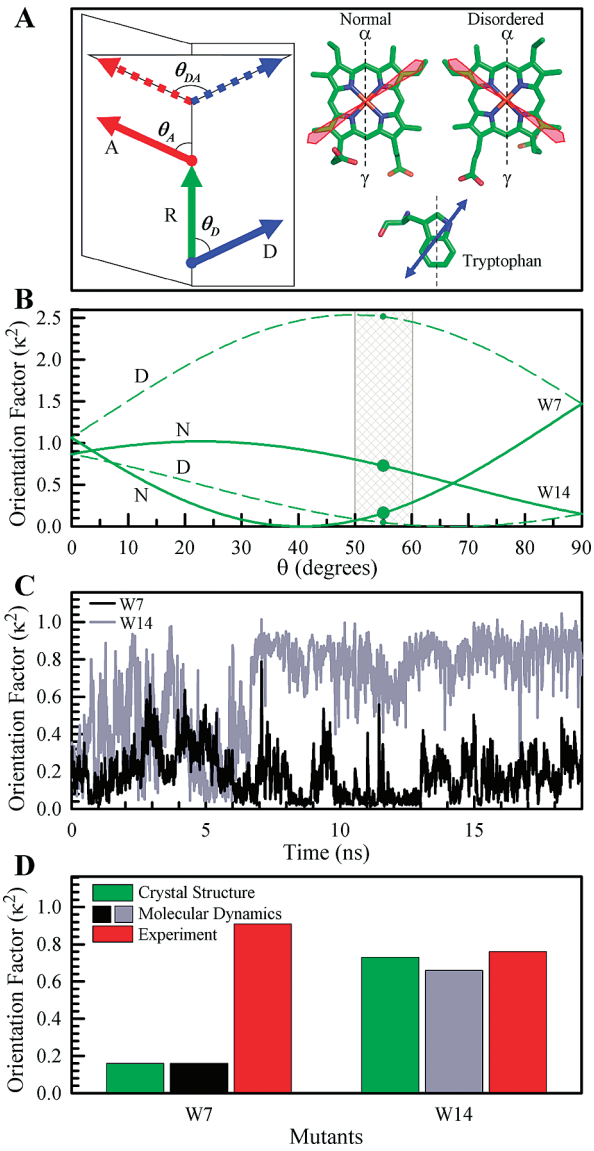

Figure 5. (A) Relative directions of transition dipole moments of the heme and tryptophan and related all angles used to calculate the orientation factor. (B) The calculated so-called "Fish" plot for both W7 and W14. Note the definition of angle θ for the normal heme (clockwise) and for the disordered heme (counter clockwise) from the $\alpha-\gamma$-meso axis as shown in panel A. (C) The calculated orientation factor distributions of a 19 ns MD trajectory simulation for W7 and W14. Note significant fluctuations observed for both W7 and W14. (D) A comparison of the orientation factors for W7 and W14 obtained from X-ray crystal structure, MD simulations and experimental measurements. Note an excellent agreement for W14 and a drastic difference for W7.

was observed by NMR[54] and has an opposite direction (Figure 5A). The calculated diagram, so-called "Fish" plot, is shown in Figure 5B for both W7 and W14, consistent with the previous calculations.[39]

For W14, we obtained the κ^2 values of 0.73 for the normal heme and nearly 0 for the disordered heme at 55° (Figure 5B) from the protein crystal structure. In heme proteins, the normal heme is dominant.[54] The observed experimental κ^2 value of 0.76 is in excellent agreement with the X-ray structure prediction of 0.73 (Table 1), indicating that at room temperature the local structure around W14 in solution is similar to the X-ray crystal structure. The W14 participates in the packing of the hydrophobic core of Mb, and this observation shows large rigidity of the core region. For the disordered heme, the κ^2 value is nearly zero and thus the RET does not occur or is extremely slow. Thus, the observed 10−20% long nanosecond component in W14 holoMb is mainly from the disordered heme holoMb although the trace apoMb might appear in the holoMb solution. As shown in our previous studies,[41] W14 can still wobble slowly in a small cone of 15° in the hydrophobic core region in 164 ps. We performed MD simulations, following our previous procedures,[55] in room temperature for the normal heme and examined the local structure fluctuations. After 1 ns equilibrium, we took a 19 ns equilibrated trajectory and calculated the orientation factor as shown in Figure 5C. Although the fluctuation of κ^2 is huge from 0 to 1, the averaged κ^2 value over 19 ns is about 0.66, surprisingly consistent with both the X-ray structure and experimental results (Figure 5D and Table 1). However, using the κ^2 and r distributions from 19 ns MD simulations, we obtained a wide distribution of energy transfer rates and cannot produce a single-exponential decay of the RET dynamics at all. We believe that MD simulations produce a too flexible protein structure as we also pointed out elsewhere.[41,56]

For W7, the results are different. From Figure 5B, we obtained the κ^2 values of 0.16 for the normal heme and 2.5 for the disordered heme at 55°. The 19 ns MD trajectory gives a surprising result of the same κ^2 value of 0.16 for the normal heme, although the fluctuation ranges from 0 to 0.6 (Figure 5C). However, the experimental result is 0.91 and significantly different. The same results from both X-ray structure and MD simulations only indicate that the local structure in MD simulations could be trapped in the substates of the X-ray structure at a local energy minimum because the structure in MD simulations originally starts from the X-ray structure. Thus, the equilibrium structure in MD simulations under room temperature in solution is a serious issue as observed here even though a long nanosecond relaxation process has been performed from the original X-ray structure, by gradually raising temperature. Clearly, the local structure under room temperature in solution is different from the local X-ray or MD simulated structures. The crystallization and packing could change the structure of the flexible region and, for W7 near the N terminal, the structure is more flexible than that around the buried W14. Thus, the observed dramatic difference does result from the local flexibility and the local conformation around W7 is easier to fluctuate. Because we do not have the correct local structure of W7, we cannot calculate the correct "Fish" plot for both the normal and disordered heme forms. This prevents us from further estimating the time scale of the RET in the disordered heme. However, we only observed a single-exponential decay of 111 ps for the RET with nearly no long nanosecond component (<1−3%). Such experimental results clearly indicate that the minor contribution of the disordered heme may have the similar RET dynamics as for the dominant normal heme, resulting in an apparent single-exponential decay, or the disordered heme percentage in the mutant of W14Y (W7) is negligible.

C. Nonequilibrium Dynamics and Conformational Flexibility. From all RET studies above, we are able to reveal the local dynamic heterogeneity and conformational flexibility from examination of the fluorescence transient behavior with single- or multiple-exponential decays and of the related orientation factors. For a given non-single-exponential decay of the RET dynamics in heme proteins, we need to consider three possibilities: (1) the local dynamic heterogeneity; (2) the changing J values due to nonequilibrium effect; and (3) the different normal and disordered heme forms. For case (1), the significant local dynamic heterogeneity would have different κ^2 values and result

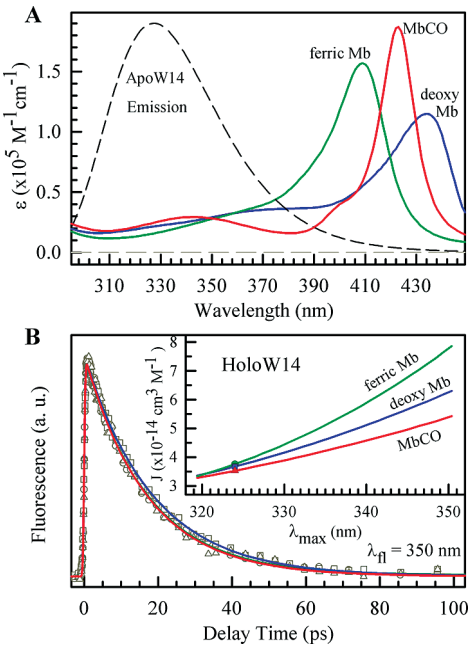

Figure 6. (A) Absorption extinction coefficients for three states of Mb (ferric, deoxy, and CO bound) of a typical tryptophan mutant (W14) with an emission spectrum from apoMb. (B) Normalized, femtosecond-resolved fluorescence transients of W14 in three states gated at the red side of the emission peak (350 nm). Note the nearly same energy transfer dynamics in these three states. In the inset are shown the spectral overlap integrals of the three states of W14 with the different emission peaks shifting from 320 to 350 nm assuming the same emission profile.

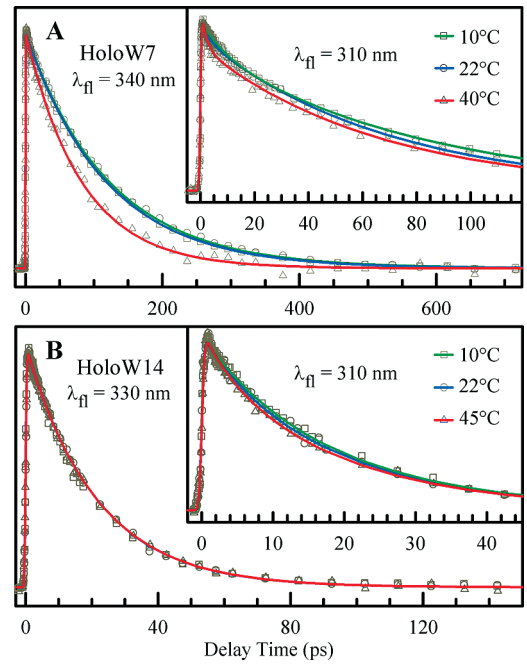

Figure 7. Normalized, femtosecond-resolved fluorescence transients show temperature dependence of the resonance energy transfer for W7 (A) and W14 (B) in holoMb. All transients are gated around the emission peak for W7 at 340 nm and W14 at 330 nm. Also shown in the inset are the transients gated at the blue side of the emission at 310 nm to examine the changes of solvation dynamics. Note that there is no change of the energy transfer dynamics at all for W14 from 10 to 45 °C but, for W7, at 40 °C it clearly becomes faster.

in the fluorescence transients with multiple-exponential decays or a stretched-single-exponential decay. For case (3), as long as we know the X-ray structure, we can calculate the "Fish" plot for two heme forms and we at most have double-exponential decays but with the dominant normal heme form.

For case (2), we need to carefully examine the relative time scales of solvation relaxation and RET dynamics and such solvation processes induce fluorescence spectrum shifts and cause the changing of J values with time. Figure 6 shows our further examination of the J values for three heme states of W14 in ferric Mb, deoxy Mb and MbCO. Figure 6A shows the three-state holoMb absorption curves and apoMb fluorescence emission of W14. Assuming to keep the fluorescence profile and shift the emission peak from 320 to 350 nm, the changing profiles of J values are shown in inset of Figure 6B. The ferric Mb has the largest value and the MbCO has the smallest value at each wavelength due to their absorption coefficients between 350 and 410 nm. Clearly, with the emission peak shifting to the longer wavelength, the J value for each heme state becomes larger and larger and the J values for three states become more and more different. Thus, for ferric Mb the J values could be more than doubled when the emission peak shifts from 320 to 350 nm and thus the RET rate could also be enhanced by two times. As we discussed above, the emission peak of W14 in holoMb for the RET is about 324 nm and thus the three J values are very close. Figure 6B shows the RET dynamics in three states with nearly the same time scale of 22 ps, consistent with the similar three J values. The slightly slower RET dynamics in deoxy Mb could result from the slightly different κ^2 value in this iron Fe^{2+} five-coordination state because the planar heme is distorted and the heme transition dipole could be changed. In the ferric state, the iron Fe^{3+} state has six-coordination with a ligand of H_2O[57] and in MbCO the iron Fe^{2+} state has six-coordination with a ligand of CO. The six-coordination iron is in the porphyrin plane, but the five-coordination iron is out of the porphyrin ring and the porphyrin plane could be slightly bent. It is clear that if the emission peak is close to 350 nm, the three states would have different RET rates.

From the RET measurements and the comparison of κ^2 values, we have observed that the local structure of W7 is more flexible than that of W14, although both give a similar local wobbling motion.[41] To compare the local conformation flexibility of the two sites of W7 and W14, we studied the temperature dependence of the RET dynamics in ferric state. According to eq III.1, the Q_D/τ_D, the radiation emission rate, is constant and the κ^2 term is mostly temperature sensitive due to the conformation fluctuations and leads to the change of the RET dynamics. In Figure 7A, the RET dynamics of W7 show no changes with the time scale of 111 ps for temperature at 10 and 22 °C but at 40 °C the RET dynamics becomes faster and the resulting energy-transfer time becomes 82 ps. We also show the transients at 310 nm in inset of Figure 7A and clearly the solvation (hydration) relaxation at 40 °C becomes faster, leading to a more red shift of the fluorescence spectrum and a larger J value for the RET process. However, as shown in inset of Figure 6B, the change of J values from 328 nm at 22 °C to at most 332 nm at 40 °C would not explain the faster RET dynamics and thus the local conformation clearly fluctuated more at 40 °C. For W14, from 10 to 45 °C, the RET dynamics shows no noticeable change as shown in Figure 7B (λ_f = 330 nm), although the solvation (hydration) relaxation becomes slightly faster (inset of Figure 7B and λ_f = 310 nm). Again, the local structure of W7 is shown to be more flexible than that of W14 and easily fluctuates with temperature increase. Such temperature-dependent studies of the RET dynamics provide a useful way to examine the relative flexibility and fluctuation of different local mutation structures around the protein.

IV. Conclusion

We reported here our systematic characterization of resonance energy transfer between the donor of tryptophan and the acceptor of the prosthetic heme group in myoglobin to develop a novel intrinsic energy-transfer pair as a molecular ruler in heme proteins to study local conformation fluctuations. With site-directed mutation, we designed four tryptophan mutants along the A-helix of myoglobin with each mutant containing only a single tryptophan−heme energy-transfer pair. With femtosecond resolution, we observed, even at separation distances of 15−25 Å, ultrafast energy transfer in tens to hundreds of picoseconds. On these time scales, the donor and acceptor cannot be randomized and thus the averaged value of 0.67 for the orientation factor, a key parameter in the Förster energy-transfer equation, cannot be used. The orientation factor is usually restricted in most proteins as shown here. Thus, the resonance energy transfer is highly orientation-factor dependent. By direct measurement of such energy transfer, we can use the derived orientation factors to examine local structures and fluctuations. We found that the local protein structure in loose regions or near terminals in solution can be different from that in crystal as shown here for W7. With temperature perturbation, we measured the changes of energy-transfer rates at different sites of W7 and W14 in myoglobin and thus we can obtain the relative local conformational flexibility and their fluctuations.

More significantly, we observed similar time scales of the energy-transfer process as the local relaxation. With excitation of the energy donor, the local environment is in nonequilibrium and such subsequent relaxations usually take a few to hundreds of picoseconds.[40,41] Thus, the resonance energy transfer is a nonequilibrium process and, using femtosecond- and wavelength-resolved fluorescence dynamics, we determined the time scales of such energy-transfer dynamics and also elucidated the mechanism of the non-single-exponential energy-transfer dynamics caused by local dynamic heterogeneity (different κ^2 values) and/or local environment relaxation (different J values).

Acknowledgment. We thank Prof. Stephen Sligar (University of Illinois at Urbana−Champaign) for generously providing us with the myoglobin plasmid (pMB122). Also thanks to Prof. Syun-Ru Yeh (Albert Einstein College of Medicine) for the helpful discussion and Tanping Li for the help of MD simulations in Figure 5C. This work was supported in part by the National Science Foundation under Grant CHE-0748358, the Packard fellowship, the Sloan fellowship, and the endowed Robert Smith professorship.

References and Notes

(1) Henzler-Wildman, K.; Kern, D. *Nature* **2007**, *450*, 964–972.
(2) Smock, R. G.; Gierasch, L. M. *Science* **2009**, *324*, 198–203.
(3) Kao, Y.-T.; Saxena, C.; Wang, L.; Sancar, A.; Zhong, D. *Proc. Natl. Acad. Sci. U.S.A.* **2005**, *102*, 16128–16132.
(4) Carter, D. C.; Ho, J. X. *Adv. Protein Chem.* **1994**, *45*, 153–203. He, X. M.; Carter, D. C. *Nature* **1992**, *358*, 209–215. Curry, S.; Mandelkow, H.; Brick, P.; Franks, N. *Nat. Struct. Biol.* **1998**, *5*, 827–835. Zunszain, P. A.; Ghuman, J.; Komatsu, T.; Tsuchida, E.; Curry, S. *BMC Struct. Biol.* **2003**, *3*, 6.
(5) Qiu, W.; Zhang, L.; Okobiah, O.; Yang, Y.; Wang, L.; Zhong, D.; Zewail, A. H. *J. Phys. Chem. B* **2006**, *110*, 10540–10549.
(6) Frederick, K. K.; Marlow, M. S.; Valentine, K. G.; Wand, A. J. *Nature* **2007**, *448*, 325–329. Lee, A. L.; Kinnear, S. A.; Wand, A. J. *Nat. Struct. Mol. Biol.* **2000**, *7*, 72–77.
(7) Junker, J. P.; Ziegler, F.; Rief, M. *Science* **2009**, *323*, 633–637.
(8) Huse, M.; Kuriyan, J. *Cell* **2002**, *109*, 275–282.
(9) Hanson, J. A.; Duderstadt, K.; Watkins, L. P.; Bhattacharyya, S.; Brokaw, J.; Chu, J.-W.; Yang, H. *Proc. Natl. Acad. Sci. U.S.A.* **2007**, *104*, 18055–18060.
(10) Lu, H. P.; Xun, L.; Xie, X. S. *Science* **1998**, *282*, 1877–1882.
(11) Palmer, A. G. *Chem. Rev.* **2004**, *104*, 3623–3640.
(12) Callender, R.; Dyer, R. B. *Chem. Rev.* **2006**, *106*, 3031–3042.
(13) Zang, C.; Stevens, J. A.; Link, J. J.; Guo, L.; Wang, L.; Zhong, D. *J. Am. Chem. Soc.* **2009**, *131*, 2846–2852.
(14) Zhong, D.; Pal, S. K.; Zhang, D.; Chan, S. I.; Zewail, A. H. *Proc. Natl. Acad. Sci. U.S.A.* **2002**, *99*, 13–18.
(15) Callender, R. *Curr. Opin. Struct. Biol.* **2002**, *12*, 628–633.
(16) Ballew, R. M.; Sabelko, J.; Gruebele, M. *Proc. Natl. Acad. Sci. U.S.A.* **1996**, *93*, 5759–5764.
(17) Du, D.; Zhu, Y.; Huang, C.-Y.; Gai, F. *Proc. Natl. Acad. Sci. U.S.A.* **2004**, *101*, 15915–15920.
(18) Pascher, T.; Chesick, J. P.; Winkler, J. R.; Gray, H. B. *Science* **1996**, *271*, 1558–1560.
(19) Jones, C. M.; Henry, E. R.; Hu, Y.; Chan, C.; Luck, S. D.; Bhuyan, A.; Roder, H.; Hofrichter, J.; Eaton, W. A. *Proc. Natl. Acad. Sci. U.S.A.* **1993**, *90*, 11860–11864.
(20) Lu, H. S. M.; Volk, M.; Kholodenko, Y.; Gooding, E.; Hochstrasser, R. M.; DeGrado, W. F. *J. Am. Chem. Soc.* **1997**, *119*, 7173–7180.
(21) Kumita, J. R.; Smart, O. S.; Woolley, G. A. *Proc. Natl. Acad. Sci. U.S.A.* **2000**, *97*, 3803–3808.
(22) Schenkl, S.; van Mourik, F.; van der Zwan, G.; Haacke, S.; Chergui, M. *Science* **2005**, *309*, 917–920.
(23) Cohen, B. E.; McAnaney, T. B.; Park, E. S.; Jan, Y. N.; Boxer, S. G.; Jan, L. Y. *Science* **2002**, *296*, 1700–1703.
(24) Getahun, Z.; Huang, C. Y.; Wang, T.; De Leon, B.; Degrado, W. F.; Gai, F. *J. Am. Chem. Soc.* **2003**, *125*, 405–411. Suydam, I. T.; Snow, C. D.; Pande, V. S.; Boxer, S. G. *Science* **2006**, *313*, 200–204.
(25) Zhong, D.; Zewail, A. H. *Proc. Natl. Acad. Sci. U.S.A.* **2001**, *98*, 11867–11872.
(26) Doose, S.; Neuweiler, H.; Sauer, M. *ChemPhysChem* **2009**, *10*, 1389–1398.
(27) Schuler, B.; Lipman, E. A.; Eaton, W. A. *Nature* **2002**, *419*, 743–747.
(28) Ha, T. *Methods* **2001**, *25*, 78–86.
(29) Kulzer, F.; Orrit, M. *Annu. Rev. Phys. Chem.* **2004**, *55*, 585–611.
(30) Phillips, S. E. V.; Schoenborn, B. P. *Nature* **1981**, *292*, 81–82.
(31) Scholes, G. D. *Annu. Rev. Phys. Chem.* **2003**, *54*, 57–87.
(32) Speiser, S. *Chem. Rev.* **1996**, *96*, 1953–1976.
(33) Saini, S.; Srinivas, G.; Bagchi, B. *J. Phys. Chem. B* **2009**, *113*, 1817–1832.
(34) Fontaine, M.; Jameson, D.; Alpert, B. *FEBS Lett.* **1980**, *116*, 310–314.
(35) Brunet, J. E.; Gonzalez, G. A.; Sotomayor, C. P. *Photochem. Photobiol.* **1983**, *38*, 253–254.
(36) Hochstrasser, R. M.; Negus, D. K. *Proc. Natl. Acad. Sci. U.S.A.* **1984**, *81*, 4399–4403. Henry, E. R.; Eaton, W. A.; Hochstrasser, R. M. *Proc. Natl. Acad. Sci. U.S.A.* **1986**, *83*, 8982–8986. Janes, S. M.; Holtom, G.; Ascenzi, P.; Brunori, M.; Hochstrasser, R. M. *Biophys. J.* **1987**, *51*, 653–660.
(37) Bismuto, E.; Irace, G.; Gratton, E. *Biochemistry* **1989**, *28*, 1508–1512.
(38) Willis, K. J.; Szabo, A. G.; Zuker, M.; Ridgeway, J. M.; Alpert, B. *Biochemistry* **1990**, *29*, 5270–5275.
(39) Gryczynski, Z.; Tenenholz, T.; Bucci, E. *Biophys. J.* **1992**, *63*, 648–653. Gryczynski, Z.; Fronticelli, C.; Tenenholz, T.; Bucci, E. *Biophys. J.* **1993**, *65*, 1951–1958. Gryczynski, Z.; Lubkowski, J.; Bucci, E. *Methods Enzymol.* **1997**, *278*, 538–569.
(40) Zhang, L.; Wang, L.; Kao, Y.-T.; Qiu, W.; Yang, Y.; Okobiah, O.; Zhong, D. *Proc. Natl. Acad. Sci. U.S.A.* **2007**, *104*, 18461–18466.
(41) Zhang, L.; Yang, Y.; Kao, Y.-T.; Wang, L.; Zhong, D. *J. Am. Chem. Soc.* **2009**, *131*, 10677–10691.
(42) Zhang, L.; Kao, Y.-T.; Qiu, W.; Wang, L.; Zhong, D. *J. Phys. Chem. B* **2006**, *110*, 18097–18103.
(43) Springer, B. A.; Sligar, S. G. *Proc. Natl. Acad. Sci. U.S.A.* **1987**, *84*, 8961–8965.
(44) Sirangelo, I.; Malmo, C.; Casillo, M.; Irace, G. *Eur. J. Biochem.* **2000**, *267*, 3937–3945.
(45) Teale, F. W. J. *Biochim. Biophys. Acta* **1959**, *35*, 543–545.
(46) Qiu, W.; Li, T.; Zhang, L.; Yang, Y.; Kao, Y.-T.; Wang, L.; Zhong, D. *Chem. Phys.* **2008**, *350*, 154–164.
(47) Li, D.; Stuehr, D. J.; Yeh, S.-R.; Rousseau, D. L. *J. Biol. Chem.* **2004**, *279*, 26489–26499.
(48) Andrews, D. L., Demidov, A. A., Eds.; *Resonance Energy Transfer*; John Wiley and Sons: Chichester, England 1999.
(49) Knox, R. S.; van Amerongen, H. *J. Phys. Chem. B* **2002**, *106*, 5289–5293. Moog, R. S.; Kuki, A.; Fayer, M. D.; Boxer, S. G. *Biochemistry* **1984**, *23*, 1564–1571.
(50) Kirby, E. P.; Steiner, R. F. *J. Biol. Chem.* **1970**, *245*, 6300–6306. Irace, G.; Balestrieri, C.; Parlato, G.; Servillo, L.; Colonna, G. *Biochemistry* **1981**, *20*, 792–799.
(51) Tcherkasskaya, O.; Bychkova, V. E.; Uversky, V. N.; Gronenborn, A. M. *J. Biol. Chem.* **2000**, *275*, 36285–36294.

(52) Meech, S. R.; Phillips, D.; Lee, A. G. *Chem. Phys.* **1983**, *80*, 317–328.

(53) Yamamoto, Y.; Tanaka, J. *Bull. Chem. Soc. Jpn.* **1972**, *45*, 1362–1366.

(54) La Mar, G. N.; Davis, N. L.; Parish, D. W.; Smith, K. M. *J. Mol. Biol.* **1983**, *168*, 887–896. La Mar, G. N.; Toi, H.; Krishnamoorthi, R. *J. Am. Chem. Soc.* **1984**, *106*, 6395–6401.

(55) Li, T.; Hassanali, A. A.; Kao, Y.-T.; Zhong, D.; Singer, S. J. *J. Am. Chem. Soc.* **2007**, *129*, 3376–3382. Hassanali, A. A.; Li, T.; Zhong, D.; Singer, S. J. *J. Phys. Chem. B* **2006**, *110*, 10497–10508.

(56) Zhong, D. Hydration Dynamics and Coupled Water-Protein Fluctuations Probed by Intrinsic Tryptophan. In *Advances in Chemical Physics*; Rice, S. A., Ed.; John Wiley & Sons, Inc.: Hoboken, NJ, 2009; Vol. 143, Chapter 3, pp 83−149.

(57) Rajarathnam, K.; La Mar, G. N.; Chiu, M. L.; Sligar, S. G.; Singh, J. P.; Smith, K. M. *J. Am. Chem. Soc.* **1991**, *113*, 7886–7892. Takano, T. *J. Mol. Biol.* **1977**, *110*, 569–584.

JP910013F